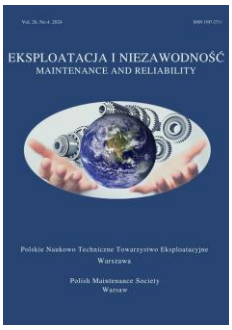

Eksploatacja i Niezawodnosc – Maintenance and Reliability

Volume 26 (2024), Issue 4

journal homepage: http://www.ein.org.pl

Article citation info:
Ferdynus M, The influence of an innovative trigger obtained by zonal appropriate annealing of the walls in a columnar passive energy absorber on the achieved crashworthiness indicators - experimental study, Eksploatacja i Niezawodnosc – Maintenance and Reliability 2024: 26(4) http://doi.org/10.17531/ein/191692

The influence of an innovative trigger obtained by zonal appropriate annealing of the walls in a columnar passive energy absorber on the achieved crashworthiness indicators - experimental study

Indexed by: Web of Science Group

Mirosław Ferdynus[a,*]

[a] Machine Design and Mechatronics, Lublin University of Technology, Poland

Highlights

- Innovative trigger in energy absorber, extremely simple to make and does not require specialized instrumentation has been demonstrated.
- The method of making a zone-annealed trigger and a classic author's trigger with spheroidal embossing has been shown.
- The methodology of experimental tests leading to the crushing force-shortening characteristics and the calculation of the crashworthiness indicators was presented.
- Based on the results of experimental studies, it has been proven that the new solutions achieve extremely favorable crashworthiness indicators compared to the energyabsorber with a classic trigger.

Abstract

The crashworthiness indicators are a key parameter for assessing the effectiveness of energy absorbers and these in turn are highly dependent on the initial phase of the crumple process and triggering mechanism. In classical designs, indentations or holes are made at a specific location to improve the triggering performance, however, the effects are limited and often unsatisfactory. This paper proposes an innovative, original solution for a column energy absorber that significantly improves the triggering parameters and relies on the introduction of smooth changes in material properties along the column axis through the use of specially localized annealing and cooling with specific parameters in its manufacturing process. The veracity of the idea presented was warranted by an experiment from which the characteristics of crushing force vs. shortening were obtained, which in turn were used to calculate crashworthiness indicators. Results confirm extremely good energy-absorbing properties of the proposed solution compared to the classic ones.

Keywords

energy absorber, crashworthiness indicator, trigger, triggering mechanism, zone annealed trigger

1. Introduction

The crashworthiness indicators are a key parameter for assessing the effectiveness of energy absorbers, in particular so-called crash boxes, and these in turn are highly dependent on the initial phase of the crumple process and its triggering mechanism. In structures of this type, the achievement of certain parameters by thin-walled members constitutes their reliability in terms of the protection they should provide to the objects they secure and thus fulfill the role they are supposed to perform [23]. On the other hand, there are a lot of publications that focus indirectly on human protection through the proper design of crash test dummies, child safety seats, etc. [19, 31].

Thin-walled metal tubes are commonly used as energy absorbers. Given the fact that they are relatively inexpensive and efficient, these tubes have been quite extensively studied [4, 6, 40] and are widely used in practice. This is particularly true of columns whose cross-section is circular, square or rectangular, where the first works appeared in the 1960s but the fundamental works [2, 15, 24] were created at the turn of the century. However, over the years, columns with other cross-sectional shapes have been analysed for their properties and

(*) Corresponding author.
E-mail addresses: M. Ferdynus (ORCID: 0000-0003-0348-631X) m.ferdynus@pollub.pl,

direct applicability [5, 29], as well as multi-corner [1, 33], multi-cell [3, 7, 38] and bi-tubal [35, 41] constructions.

The behaviour of this type of structure during axial, oblique and lateral crushing has been extensively studied over the past decades. However, a very important aspect that requires further research is the triggering effect and the influence of this initial crushing phase on the whole energy absorption process and its efficiency. Some work has already been published giving due attention to this phenomenon [25, 32], however, the issue still needs to be researched and the work presented here is intended to partially fill this gap. The paper [25] analysed the effect of the placement of triggers in the form of grooves on square sections on the peak crushing force PCF. The optimum groove arrangement was obtained by introducing indentations with a spacing corresponding to the fold length accurately estimated by computer simulation. Two decades later, there was a paper published by Rai et al [32], where the results of a study on the influence of the triggering mechanism on the achieved crash force efficiency CFE, stroke efficiency SE, and specific energy absorbed SEA indicators for aluminium tubular absorbers limited to circular tubes were presented. On the basis of numerical and experimental results, it has been conclusively proven that tubes made of aluminium alloy show a better rate of SEA than those made of steel. One of the attempts in which the influence of geometric parameters of triggers on crush efficiency rates was related to this phenomenon is the article [11], where besides, a neural network was used to predict the achieved effects depending on the planned trends of changes in the aforementioned geometric parameters.

A very interesting and novel consideration of the reproducibility of experimental tests of square crash boxes is presented in the paper [17]. The study deals with the influence of the initial crush phase on the final effect of the deformation form of the specimens, in particular: the unavoidable imperfections, the appearance of cracks and other perturbations related to the propagation of the elastic wave, as was written about many years earlier [21]. The axial crushing of square crash boxes is a complex phenomenon in which the unrepeatability of tests is quite common, yet the quality of the numerical model validation carried out, for example, depends on the selection of reliable experimental tests.

In the field of crashworthiness, the considered energy absorber with an innovative trigger is positioned among the issues of functionally graded structures, where an extensive review of the work is presented in the article [37]. The change, in general terms of properties, along the vertical axis of the energy absorber can take place by changing the cross-sectional dimensions [13] or by changing the wall thickness [9, 18, 36]. It may also be the case that both are changed [26, 43].

The density of the foamed insert can also change- with very interesting results [39], however, there are very few works in which the material properties are changed along the axis of the energy absorber.

It is impossible not to mention the modern technology of tailored blanks [28], where sheets of varying strengths are obtained, the configuration of which is dedicated to achieving the planned strength effect. These sheets are either welded together before being finally formed by pressing, or patched and overlapped where a reinforcing effect is needed. In this solution, the distribution of material properties is generally stepped rather than smooth, but this is not an obstacle in applications for surface objects. However, this technology has not yet been applied to the construction of crash boxes, as it is mainly used to obtain extrusions with an optimum distribution of strength properties. However, a technology for local laser annealing of hollow sections is described, with the aim of improving their formability prior to bending in order to achieve the right geometric effect and avoid possible cracking during this operation [27]. The scale of the change in the material was not reported, only the application effect. That technology is today known under the generic term “Tailored Heat Treated Blanks ” (THTB) and, in addition to its application to steel structures, is also suitable for 6000 series aluminium alloys. Short-term heat treatment of hardenable aluminium with laser radiation leads to significant softening of the aluminium blank. Particles causing precipitation hardening are locally dissolved during the heat treatment and a quasi-solution annealing state appears. A similar effect also occurs during flame annealing, which became the matrix of the idea presented in this paper in application to a crash box.

A related idea with regard to the design of the tooling, in which it is necessary to supply heat to the place where the bending process takes place, was presented in the work of Gronostajski et al [14]. This paper also pays close attention to the quality and ingenuity of the tooling used to fabricate the test specimens, as this process is a very important aspect of the subsequent application possibilities. Even the best ideas without efficient technology for its implementation lose their relevance and have to wait for manufacturing capabilities to emerge.

The idea of obtaining an energy-absorber with similar crashworthiness properties by joining two components with different properties by a transverse laser weld (so as not to overheat) was abandoned as being more costly and not guaranteeing a satisfactory result in practice. Other reasons were also not insignificant. Aluminium alloys have poor weldability, due to their high reflectivity, low alloy viscosity and the existence of oxide layers. This leads to porosity, hot cracking in the fusion zone, reduced strength and loss of alloying elements. In the case of laser welding, the bonding that occurs is weak, yet it is necessary for the energy absorber to provide high reliability. Where welds are required, it is always preferable for them to be located along the load rather than across it [8, 34].

A similar concept of using zonal annealing of an aluminium profile to obtain an improvement in its energy-absorbing properties is presented in the work of Peixinho et al. [30], where the trigger was made by creating lines heated with a laser welder. Eight models were made for experimental testing, differing in the location of the heated lines by their number and configuration. Quasi-static and dynamic tests were conducted on the drop tower. The results of the tests were the crush force-shortening characteristics, from which the maximum crush-initiating force and the average force were obtained. It was confirmed that there was a 19% reduction in PCF force in columns with a certain heated line configuration. Other indices and parameters were not calculated. However, compared to the studies presented here, laser welding annealing changed the properties of the aluminium alloy in a very limited zone. The measured change in hardness was limited to a maximum of a few millimetres around the laser weld line on the sidewall. The effect achieved is similar to that obtained with classical solutions. The very important crash load efficiency CLE index and stroke efficiency SE and total efficiency TE were not tested, but it must be remembered that this publication is more than a decade old.

In the context of the literature study, the presented solution - the zone annealed trigger in the columnar energy absorber with its extremely favourable properties in terms of the achieved crashworthiness indicators - appears to be original, promising and will undoubtedly be the subject of further studies.

1.1. Objective and scope of the study

In classical designs, in order to improve the triggering parameters, indentations or holes are made in a specific location, which results in a certain reduction in the peak crushing force (PCF) during the crush. The manufacture of such triggers often requires the use of specialised instruments. Still, due to the limited capabilities of this method, obtained results are often unsatisfactory.

The main objective of this study is to present an innovative solution that, in particular, significantly improves the triggering parameters. It consists of introducing smooth changes in material properties along the axis of the columnar energy absorber. This effect was achieved by the application of specifically localized annealing and cooling. The change induced in material properties along the axis is invisible to the unaided eye and is reflected by the change in hardness along the axis of individual walls, a phenomenon which does not occur in non-annealed columns.

The induced change in material properties, which is particularly beneficial in terms of reducing PCF at the same time also reduces the mean crushing force (MCF) in the initial phase of crushing, resulting in a reduction of overloading in this phase making it better protect the object in terms of the reliability of the controlled crushing zone. In general, the new type of trigger definitely improves the crash load efficiency value (CLE), which is very beneficial for biomechanical reasons. The higher its value, the less overload the occupant of a vehicle equipped with this safety device becomes.

The veracity of the idea presented was confirmed by an experiment. Its methodology has been described in detail. The method of obtaining an innovative trigger is also presented, as well as the author's method of obtaining a classical trigger in the form of spheroidal embossing. The experimentally obtained characteristics of the crushing force as a function of shortening, were the basis for calculating the crashworthiness indicators. That rates are then compared with the results obtained for an energy absorber with a classical trigger in the form of indentations and for a column with the same sizes and wall thickness, but without a trigger. It is shown that the energy absorber made according to the method presented in this paper is characterized by very good parameters which are unattainable with the use of existing solutions.

1.2. Crashworthiness indicators

The key problem in the research on energy absorbers is the determination of a crush force vs. shortening (displacement) relationship. Most crashworthiness indicators are calculated based on this relationship. Some of these indicators have existed in the literature since the beginning, but it is characteristic that new ones have emerged over the years to describe the properties of energy absorbers in different aspects. The paper by Fang et al. [10] can trace this process and the evolution of terminology and designations. In this context, the work of Kotelko et al. [22] can also be considered of value. An example of a performance characteristic of an energy absorber is shown in Figure 1.1.

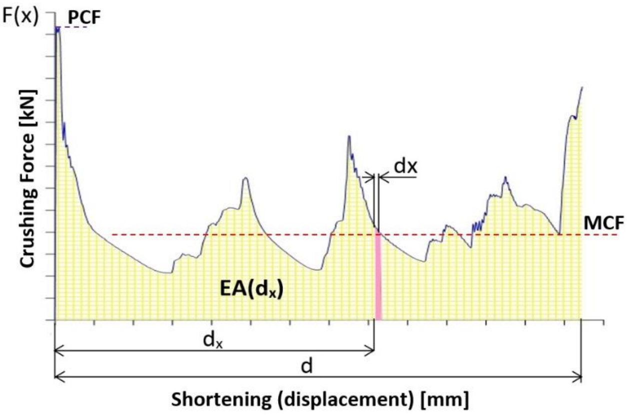

Fig. 1.1. Example of a crush force vs. shortening characteristic

The main focus of crumple zone designers is the amount of energy absorbed by the object, a measure of which is the field under crushing force and shortening characteristics (Figure 1.1). It can be seen that as the crushing process progresses, the energy absorbed by the structure increases. This energy is given by the following formula:

$$EA(d_x) = \int_0^{d_x} F(x)dx \tag{1}$$

where d_x is the crushing distance and F(x) is the crush force.

The absorbed energy is frequently given in relation to the mass unit and defined as specified energy absorbed (SEA). It is expressed as:

$$SEA = \frac{EA(d_x)}{m} \tag{2}$$

The two above-mentioned quantities (EA and SEA) do not characterize energy absorption properties but indicate the quantity of absorbed energy. An energy absorber will absorb exactly the amount of energy it is loaded with, nevertheless, if its structure is not designed for such a high load, it will be compressed and large overloads will occur in the system. Therefore, simply knowing the amount of energy absorbed, without taking into account the deformation state of the structure and its ability to absorb the next portion of energy and the effects of overloading, is highly insufficient.

There exist other measured values and indicators that describe energy absorption properties in a more comprehensive way. These include PCF and the mean crushing force (MCF) which is often denoted by P_m or P_{AVG}. These measured values and indicators are also shown in Figure 1.1. The mean crushing force is a quotient of the energy absorbed EA over the distance d_x to the value of this distance. It is expressed as:

$$MCF = \frac{EA(d_x)}{d_x} \tag{3}$$

Another key indicator is the crush load efficiency (CLE), which is related to the above quantities and is expressed a percentage ratio of the mean crush force to the peak crush force, as given in Equation (4):

$$CLE = \frac{MCF}{PCF} \cdot 100\% \tag{4a}$$

This indicator often comes in a dimensionless form and is often described as crash force efficiency (CFE).

$$CFE = \frac{MCF}{PCF} \tag{4b}$$

A reduction in PCF is highly desirable for biomechanical reasons and that this factor in itself is an important indicator of absorber properties. PCF is also an extremely important factor influencing the CLE value (formula 4a), as the influence of the type of trigger is very large as far as the denominator is concerned and negligible as far as the numerator in this relationship is concerned.

Another indicator of deformation of a structure is known as stroke efficiency (SE) and expressed as:

$$SE = \frac{U}{L_o} \tag{5}$$

where U is the crushing distance (maximum shortening), and L_o is the initial height of the energy absorber.

It is one of the basic performance indicators. An ideal structure should make it possible that stroke energy be absorbed over the entire length of the structure. Obviously, this is not 100% possible in practice; nonetheless, the higher the value of this indicator is, the more benefits this will bring.

A combination of CFE and SE in the form of product was first proposed by Hansen et al. in [35] as total efficiency (TE). Since then, this indicator has been frequently used either in a dimensionless form (6a) or as expressed in % (6b).

$$TE = CFE \times SE \tag{6a}$$

$$TE = CLE \times SE \tag{6b}$$

Since this indicator does not consider the effect of an energy absorber mass, another indicator has been introduced to compensate for this shortcoming. Zhang et al. in a study [42] proposed that TE be divided by mass, and the new thereby obtained indicator was coined as specific total efficiency (STE) and is expressed with the following formula:

$$STE = \frac{TE}{m} = \frac{CLE \times SE}{m} \tag{7}$$

All the above indicators describe the characteristics of an absorber that is used in a specific structure and made of particular material. It is then very difficult to compare characteristics of energy absorbers made of different materials. The first indicator considering the material factor was introduced by Jones [20]. It is known as structural efficiency and defined as:

$$\eta = \frac{MCF}{A \cdot \sigma_o} \tag{8}$$

where A is the cross-sectional area of the energy absorber and σ_o is the yield stress of the energy absorber material.

2. Object of the study

The object of the study was a columnar energy absorber (crash box) made from a standard 40x40 square section column with a wall thickness of 1.2 mm and a height of 200 mm. The novelty of the study lies in the way of obtaining specific properties of the energy absorber's material, these properties varying in at least half of its volume with the distance from the edge. This property was obtained by annealing an AW6063- T6 aluminium alloy column with a gas torch. This specimen was designated as AT-200 (**A**nnealed **T**rigger).

For comparison, we also fabricated an energy absorber with a trigger in the form of four spherical indentations made on the same level on the column walls. These specimens were designated by B35-g2-h30, which means that the spherical indentation reached a diameter of 35 mm on the column wall, its depth was twice the wall thickness (2.4 mm), and it was made at a height of 30 mm from the edge.

To fully illustrate the benefits of the proposed novel solution, a model of a classical column without any changes to its cross-sectional shape and material was prepared (SM-200- **SM**ooth). Examples of the above specimens are shown in Figure 2.1a-c.

Although the energy absorber with spherical indentations was partly described in [12], that study investigated a simplified model of the absorber, with only concave indentations that were easier to make. In the present study, indentations are located opposite in pairs: concave and convex. The method of making a trigger of this type on the profile (1) requires the use of specialist tooling; in addition, convex (Figure 2.2a) and concave (Figure 2.2b) indentations are made separately, and the order in which they are made and their precise location are equally important. The convex indentations are made first and then the concave ones. The novelty of this study is the process of making convex indentations, which is partly based on hydroforming but does not require the use of expensive equipment.

The tooling for making convex indentations consists of outer dies (3) and blocking plates (2). The outer dies have spherical indentations while the blocking plates are flat and protect the surfaces from deformation during the indentation-making process. The dies and plates are mounted on the profile and locked in a desired position using a clamping frame (4). After that, spacing plates and a rubber insert are put inside the column. The rubber insert must be positioned very precisely, which is ensured thanks to the appropriate height of the plate stack. The whole device is put in a hydraulic press and a piston (5) is used to exert load on the rubber insert, which undergoes upsetting and makes an indentation.

The tooling for making concave indentations is much simpler. It consists of an inner die (6) that is split in a plane perpendicular to the axis of the column. The die is positioned as required and pressure is applied to the column through a rubber insert (7).

The press force, for both concave and convex indentations, must be chosen very carefully to ensure that the indentations have the intended depth and, on the other hand, that the column does not unintentionally deform or crack at the edge.

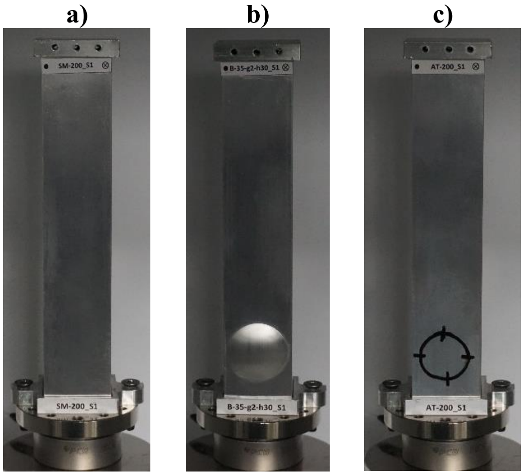

Fig. 2.1. **a)** Smooth specimen without trigger **b)** specimen with spherical indentations **c)** specimen with zone-annealed trigger.

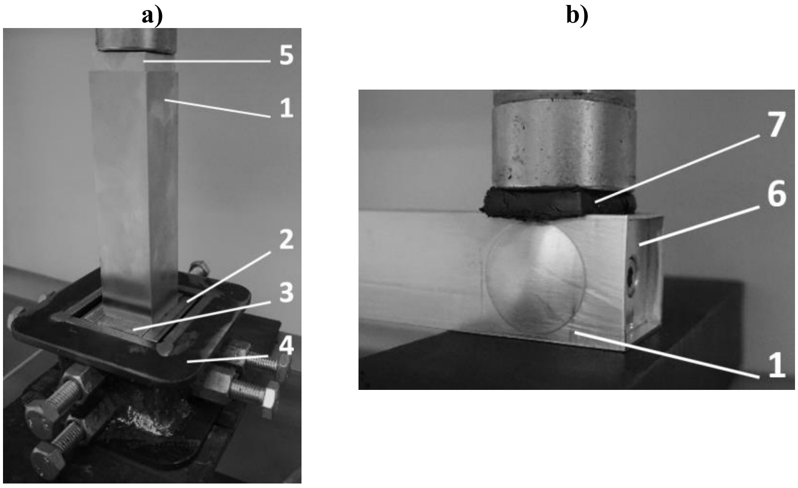

Fig. 2.2. Tooling for making spherical indentations: profile, (2)- blocking plate, (3)- outer die, (4)- clamping frame, (5)- piston, (6)- inner die, (7)- rubber insert.

2.1. Method of making a zone-annealed trigger (ZAT)

The idea of a trigger invisible to the eye is based on the properties of many aluminium alloys which, when subjected to annealing, undergo phase transformations, which results in reduced hardness of these alloys. To increase the CLE value in particular, it is crucial that this transformation should only take place only in a specified zone. If the material was modified throughout its entire volume, then the energy absorption efficiency would significantly decrease as a result of a drop in the MCF value. Thus, the enhancement of the CLE indicator should be done by reducing the PCF value while maintaining the MCF value as high as possible compared to the non-annealed columns.

To achieve a zone-specific change in material properties, the columns were subjected to the following repetitive procedure. Each wall was annealed with a propane-butane gas burner placed so that the burner axis was perpendicular to the wall and intersected the wall in its vertical axis at a distance of 30 mm. The distance of the edge of the burner from the wall being annealed was 18 mm. The annealing was run for 180 s, after which the profile was left to cool on its own. After that, another wall was subjected to annealing and cooling. During annealing, the wall reached a temperature of 380- 390 degrees Celsius, while at the bottom the temperature reached 90 degrees. The measurements were made on the wall inside the profile, the one heated by the flame. The temperature was measured using a multimeter with a K-type probe. A column during annealing is shown in Figure 2.3. It is noteworthy that the changes that occur in the material are stable and have persisted for several years suggesting that the structural changes in the aluminium alloy are permanent. The author has specimens that were annealed several years ago and their hardness has remained almost unchanged.

Fig. 2.3. Annealing of a column.

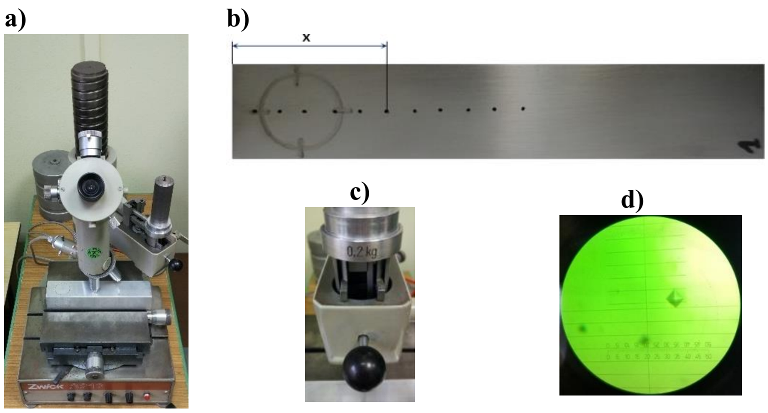

Fig .2.4. **a)** Measurement of column wall hardness **b)** column with indicated measuring points - distance x from the top edge **c)** load head **d)** microscopic view of an imprint

2.2. Results of column hardness measurements

Prior to annealing, the homogeneity of the material was assessed by measuring hardness at three randomly selected locations on each specimen. To ensure minimal interference with the surface of the specimens, hardness was measured by the Vickers method using the lowest load of 0.2 kg, where the maximum indentation depth was 0.06 mm.

Obtained hardness results are listed in Table 2.1. The mean hardness does not basically differ from that stated by the manufacturer in the specification sheet, and the standard deviation SD is small, which indicates that the tested material was fairly homogeneous before the treatment. The specimens were denoted by S1, S2, S3.

Tab. 2.1. Results of control measurements of column hardness before heat treatment

Measurement	**S1**	**S1**	**S2**
1	81.46	82.01	77.09
2	78.16	79.44	82.06
3	81.33	77.69	79.34
HV 0.2 $_{mean}$	80.32	79.71	79.50
SD	1.527	1.774	2.031

Following the heat treatment of all walls described in the previous section, control hardness measurements were made using the same Vickers HV 0.2 method. The hardness measurements were carried out in the axis of each wall, every 10 mm from the top edge, in the range from 10 mm to half the height of the column, i.e. 100 mm. Above 100 mm, the hardness value becomes stable within the hardness limits for a non-annealed column. Figure 2.4 b-d shows an example of an annealed specimen with indicated measurement locations, a specimen mounted in the Zwick 3212 hardness tester, and an example of an imprint as seen under the microscope. Please note that the top edge of the wall relative to which the hardness measurement points are positioned refers to the time of annealing. However, during the experiment, this edge becomes the bottom edge.

The specimens modified by annealing were denoted by AT-200 with extensions S1, S2, S3. The hardness results obtained are shown in Tables 2.2- 2.4 in columns 2-5. Columns 6 and 7 give the mean hardness for four walls corresponding to a given distance x as well as the standard deviation which is a measure of the annealing-induced homogeneity of the structure. The mean hardness HV 0.2 $_{mean}$ is a good reference for predicting both the size of the zone where the material underwent a change after annealing and the extent of this change. The size of this zone and the distribution of hardness along the column axis will affect the behaviour of the energy absorber during the crushing process. The values of the mean Vickers hardness HV 0.2 are plotted in Figure 2.5. It can be observed that the curves generated for the three specimens are similar. At a distance of up to 30 mm from the edge of the column the hardness ranges from about 36 to 38 HV and then, as x increases, the hardness value increases more and more rapidly to become stable near x= 90-100 mm, i.e. half the height of the column, at a level of about 79-80 HV (approximate wall hardness of the unannealed column).

Tab. 2.2. Hardness of every wall together with its mean values and standard deviations for AT-200_S1.

AT-200_S1	Wall number				**HV 0.2 $_{mean}$**	**SD**
Distance **x**	1	2	3	4		
10 mm	38.62	37.46	35.21	34.12	36.35	1.78
20 mm	38.72	36.55	36.13	35.21	36.65	1.29
30 mm	40.22	38.89	37.42	36.44	38.24	1.44
40 mm	43.13	42.24	40.86	39.95	41.55	1.23
50 mm	51.02	49.66	48.43	47.07	49.05	1.46
60 mm	62.79	61.54	60.08	57.55	60.49	1.95
70 mm	72.35	71.15	70.11	68.57	70.55	1.39
80 mm	78.68	77.96	75.5	74.98	76.78	1.57
90 mm	81.52	79.44	79.14	77.85	79.49	1.32
100 mm	81.97	81.13	79.69	78.62	80.35	1.29

SD – standard deviation

Tab. 2.3. Hardness of every wall together with its mean values and standard deviations for AT-200_S2.

AT-200_S2	Wall number				**HV0.2mean**	**SD**
Distance **x**	1	2	3	4		
10 mm	38.52	38.46	36.89	34.61	37.12	1.59
20 mm	39.31	37.99	36.69	35.65	37.41	1.37
30 mm	40.55	39.45	37.9	36.81	38.68	1.43
40 mm	43.32	41.49	40.15	39.85	41.20	1.37
50 mm	49.87	48.93	48.22	45.98	48.25	1.44
60 mm	61.85	60.98	58.23	57.11	59.54	1.94
70 mm	70.43	69.35	67.83	66.79	68.60	1.39
80 mm	77.05	76.06	74.83	73.75	75.42	1.25
90 mm	80.26	79.16	77.73	76.06	78.30	1.58
100 mm	81.17	79.66	78.36	78.34	79.38	1.16

SD – standard deviation

Tab. 2.4. Hardness of every wall together with its mean values and standard deviations for AT-200_S3.

AT-200_S3	Wall number				**HV0.2mean**	**SD**
Distance **x**	1	2	3	4		
10 mm	38.47	38.42	36.29	34.63	36.95	1.60
20 mm	38.19	38.11	35.74	35.03	36.77	1.41
30 mm	39.88	37.22	36.33	35.24	37.17	1.72
40 mm	43.28	40.58	38.82	37.93	40.15	2.04
50 mm	49.06	47.04	46.9	45.51	47.13	1.27
60 mm	59.71	57.92	57.08	56.41	57.78	1.24
70 mm	70.51	69.75	68.23	66.89	68.85	1.40
80 mm	77.65	76.52	75.05	74.05	75.82	1.38
90 mm	80.72	79.43	78.23	76.63	78.75	1.51
100 mm	80.96	79.85	79.34	78.87	79.76	0.78

SD – standard deviation

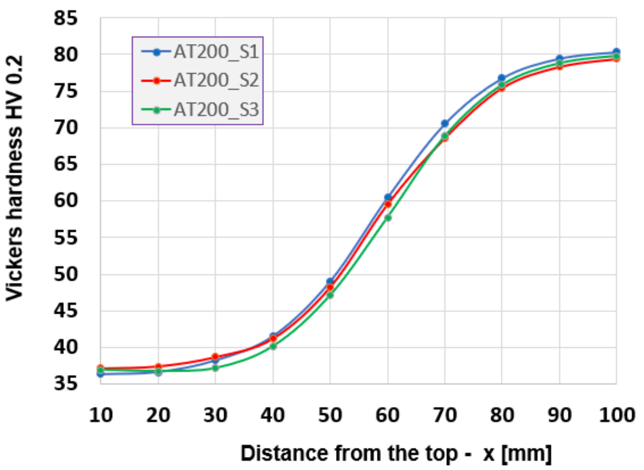

Fig. 2.5. Mean wall hardness HV 0.2 versus the distance from the top edge of the specimens.

3. Experimental research

In order to verify indisputably the advantages of the innovative solution, experimental tests of progressive crushing were carried out on three models: one with a zone-annealed trigger (ZAT), one with a classical trigger in the form of spherical indentations, and one without any trigger for reference. The purpose of the study is to determine the crushing force vs. shortening characteristic that can be used to calculate some crashworthiness indicators described in detail in Section 1.2.

3.1. Test stand and experimental research method

Experiments were conducted on the Instron Ceast 9350 HES drop tower, which is shown in Figure 3.1a. The device consists of three main units: test chamber A (Fig. 3.1c), drop track module B (Fig. 3.1b), drop energy boost system C. Data from the measuring sensors are sent to a data acquisition control module that communicates with the main computer. The Ceast-View software makes it possible to control the drop process and acquire measurement data.

In addition, the test stand was provided with a high-speed camera, Phantom Miro M310 (Fig 3.1d). The camera was equipped with an image analysis system that allowed not only to examine successive stages of deformation of the specimens, but also to obtain characteristics of tup displacement /velocity/delay as a function of time, which made it possible to verify data acquired directly from the drop tower.

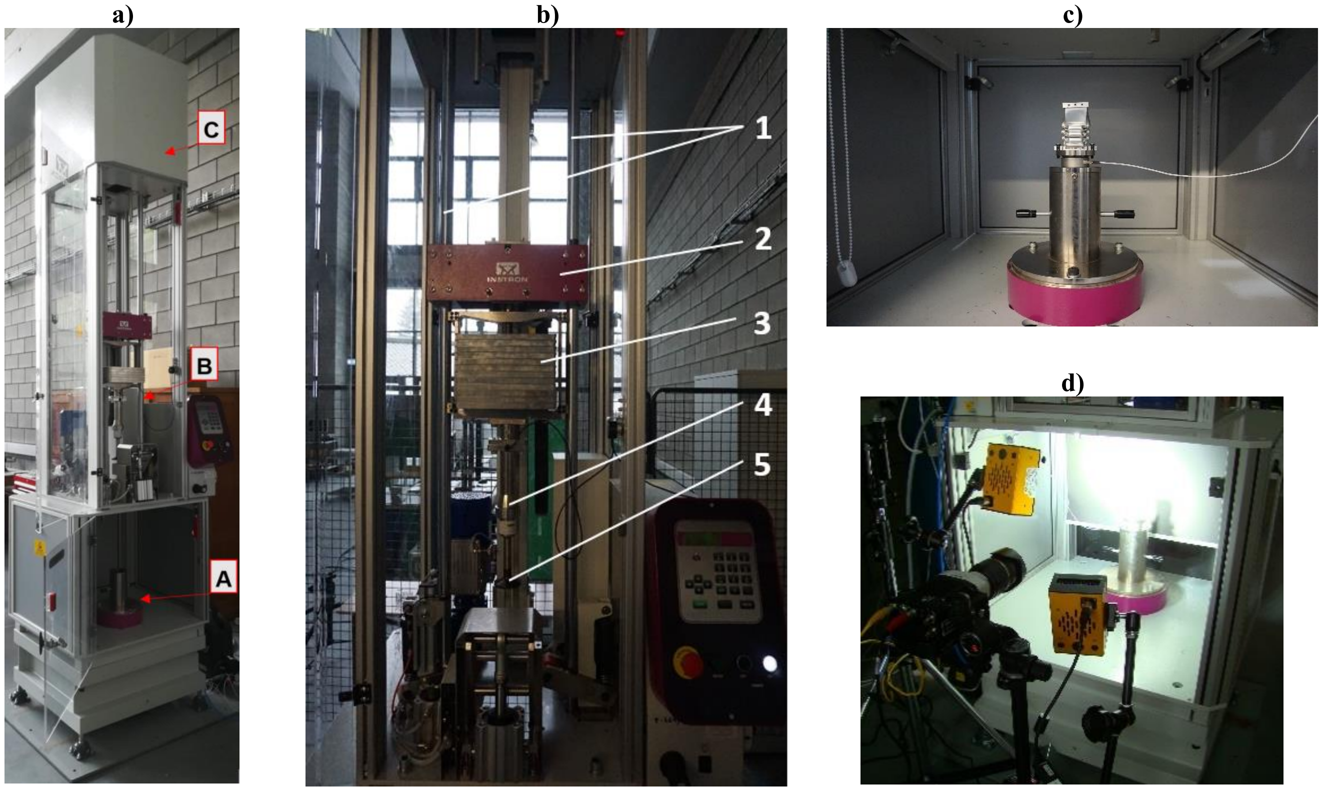

Fig. 3.1. **a)** General view of Instron- Ceast 9350HES drop tower **b)** drop track module **c)** test chamber **d)** stand with a high-speed camera during testing.

Inside the test chamber is mounted a universal worktable with a piezoelectric load sensor ICP-200C50 from PCB, provided with a plate to which test specimens are attached. The drop track module contains practically the entire work system which consists of: guide rails (1), crosshead (2), frame with weights (3) to which is attached a tup (4) with an interchangeable tip (5), whose shape depends on the type of test.

The tup can be instrumented or not, i.e. it can have an integrated force sensor or not. The system for increasing drop impact energy is based on the energy stored in two springs tensioned by a lead screw that is driven by an electric motor via a worm gear. This energy is released at the appropriate moment by releasing the bolts when a signal is sent by the control system. The degree of spring tension is also selected by the control system depending on the drop impact energy.

The key component of the main unit is an adjustable crosshead that is driven by a lead screw and moves vertically along two guide rails. Just before the actual test, the crosshead travels down until the tup comes into contact with the specimen in order to determine the zero position from which it measures the free impact drop height in tests conducted without springs. This parameter is also of key importance when tests are conducted with the impact energy-enhancing springs. The impact velocity sensor is set in the zero position to measure impact velocity just before the tup hits the specimen.

The special frame is suspended from the crosshead, which also moves along the guide rails and is fixed in the crosshead on a vertical pin, which is locked by a catch. The desired number of weights are mounted in the frame. Their weight and declared impact energy determine the impact velocity to be generated by the machine. The program will inform you whether the selected set of parameters (weight, velocity) is attainable and whether the impact drop impact will be free or will require using the drop energy boost system.

If the preset impact velocity is unattainable in a free drop test (>4.65 m/s), which is generally the case with drop tests conducted with an impact energy greater than 757 J, the system will automatically use the drop energy boost system. The crosshead together with the weights frame travels to the maximum top position and the latches for immobilizing the crosshead are locked; after that, the spring system is tightened with the force selected such to apply an impact with the preset energy. After releasing the catch connecting the crosshead to the frame with weights and tup, the crosshead is ejected downwards along the guide rails. An impact velocity sensor confirms whether the preset impact velocity has been reached. This information is used to periodically adjust/calibrate the impact energy control module.

All tests were conducted with an impact energy of E=1.482 kJ. This energy was obtained with a total mass of the frame-weights-tup set of m=70.825 kg and an impact velocity of v=6.47 m/s. Data about time, tup displacement and impact-generated force were collected and visualized in the Ceast View system and then exported to a spreadsheet. At the same time, the impact process was recorded with a Phantom Miro high-speed camera to observe individual stages of deformation of the structure, which – in addition to broadening the state of knowledge – will allow verification of the quality of numerical models in the future. The captured images were also examined using specialist software provided to the camera for the displacement of a selected point (the cross on the top sticker) to confirm the data acquired from the drop tower.

3.2. Experimental results

The main result of the test is to obtain the characteristics of the crushing force in relation to shortening, from which the crashworthiness indicators are determined. Images captured by the high-speed camera make it possible to examine individual stages of deformation. The successive stages of the deformation process for the energy absorbers are shown in Figures 3.2- 3.4, while examples of deformed specimens mounted on the workbench are shown in Figure 3.5.

SM-200_S1

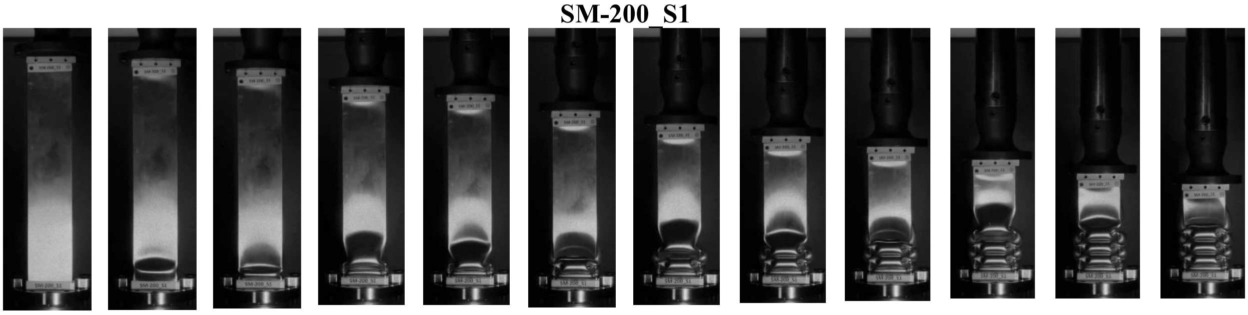

Fig. 3.2. Successive stages of deformation of energyabsorber with smooth walls (without trigger).

B-35-g2-h30_S1

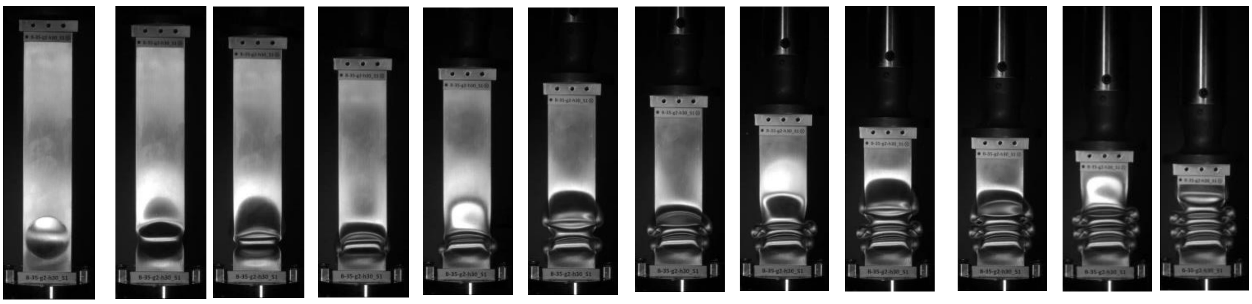

Fig. 3.3. Successive stages of deformation of energyabsorber with spherical indentation trigger.

AT-200_S1

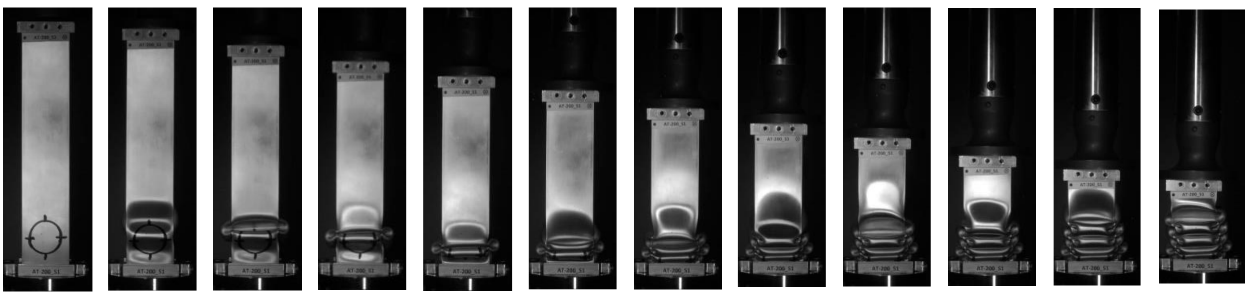

Fig. 3.4. Successive stages of deformation of energyabsorber with innovative zone- annealed trigger.

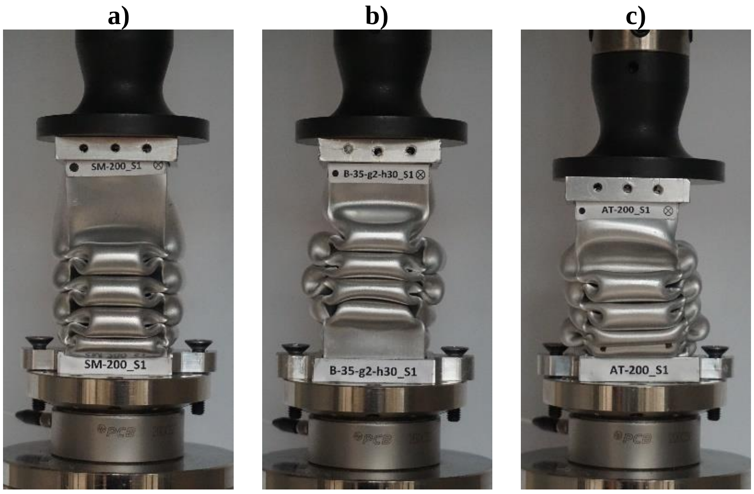

Fig. 3.5. Deformed specimens after testing: a) smooth one b) with spherical indentations c) with zone-annealed trigger (ZAT)

In all cases analysed, the deformation process is similar. It starts at the bottom of the specimens, where the trigger is located. The results obtained from two tests for the smooth column (SM model) show that despite the absence of a trigger, the crushing process started at the bottom, although previous experimental studies showed that there were case when the failure process started at the top. Individual frames of the film show the formation of successive folds until the final deformation mode is achieved. For the energy absorber with a zone-annealed trigger, it can be seen that the folds are arranged more tightly in the initial phase of crushing, which is due to the changes in material properties in at least half of the column volume. It is also worth highlighting that the energy absorption process occurs over a longer distance (which is generally beneficial).

As previously mentioned, the experimental result obtained from drop-tower testing provides the relationship between the crushing force from the piezoelectric sensor and time and displacement. The characteristics of crushing force as a function of shortening shown in Figures 3.6-3.8, which are the results of the experimental tests on the three types of specimens, were used to calculate crashworthiness indicators. Without the determination of these characteristics, over the entire crush range of the structure, up to the absorption of the entire drop energy, the calculation of reliable indicator values would have been impossible.

It can be observed that, compared to the smooth specimens and those with the classical trigger, the PCF value decreased spectacularly in the new solution. Due to the fact that all specimens were impacted with the same drop energy, it is clear that the areas under the curves are very similar and close to the drop energy (a certain portion of heat is generated).

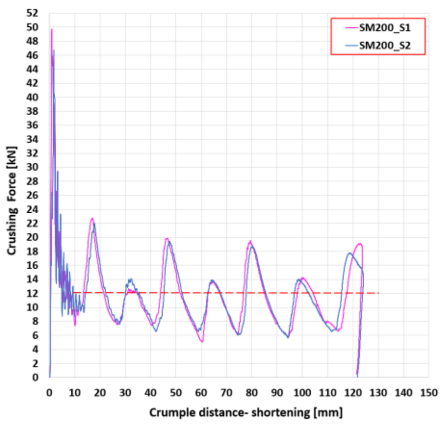

Fig.3.6. Crushing force vs shortening diagram for smooth specimens without triggers.

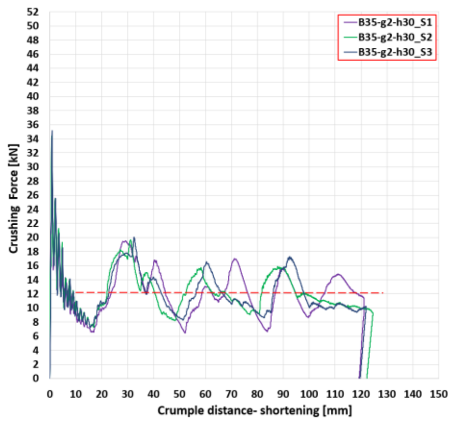

Fig.3.7. Crushing force vs shortening diagram for specimens with spherical indentations.

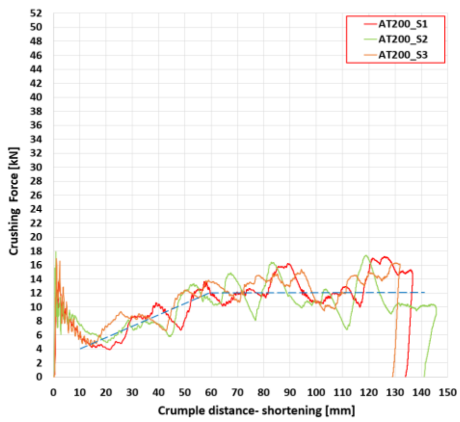

Fig.3.8. Crushing force vs shortening diagram for specimens with innovative zone-annealed triggers.

It is also worth noting that, if the initial stage of crushing is omitted, the mean crush force as a function of displacement is a roughly constant value. That is why, in Figures 3.6 and 3.7 this stage is marked with a horizontal dash line at a height approximately equal to the MCF value of about 12 kN. It can be seen that the actual crush force oscillates around this line. In the innovative solution, after the initial phase of crushing, the crush force oscillates around a line that runs at an acute angle first and then stabilizes as a horizontal line at a height of about 12 KN.

For comparison reasons, the results obtained for selected individual specimens from each group are compiled and given in Figure 3.9. Energy absorber with innovative zone-annealed trigger absorbs energy over a longer distance (10 to 18%). This is because it has poorer strength properties in a certain zone, so it absorbs less energy at this stage of the crushing process than the other columns. Thus, the energy that has not been absorbed in the initial phase is used to deform the specimen in the final stage of crushing, which, assuming constant energy drop, has the effect of clearly extending the crush distance. The extension of the crushing distance with the drop energy maintained constant generally leads to lower overloads, which is generally desired.

As mentioned, the experimental characteristics were used to determine the crashworthiness indicators using the equations presented in Section 1.2. The obtained values of these indicators are listed in Table 3.1. The use of the innovative ZAT solution results in approx. 50% reduction in the PCF value compared to that obtained for the classical trigger column, while in relation to the smooth column – this difference increases to 64%.

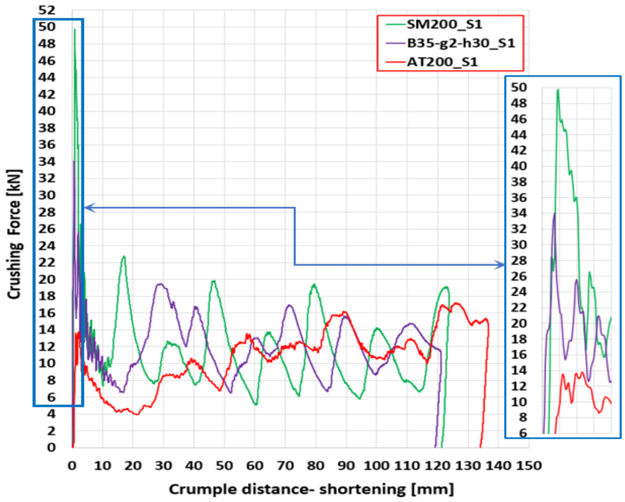

Fig.3.9. Crushing force vs shortening diagram for selected specimens (one from each group).

A spectacular increase can also be observed for the CLE indicator, which is associated with a drastic reduction in PCF. The CLE value increased by 71.25% compared to the column with a classic trigger and by up to 147.3% compared to the smooth column. The SE value increased by 15% and 12.5%, respectively. The observed significant increases in CLE and SE result in a huge increase in the TE value, which is the product of these indicators. This indicator increased by 96% compared to the column with a classical trigger and by 178% compared to the smooth column. Changes in the crashworthiness indicators obtained for the specimens with a classical trigger and with ZAT compared to the smooth column are given in Table 3.2.

Tab. 3.1. Crashworthiness indicators and maximum shortening.

Model	PCF [kN]	U_{max} [mm]	MCF [kN]	CLE [%]	SE [-]	TE [%]
SM-200_S1	49.784	123.71	11.948	24.00	0.6185	14.85
SM-200_S2	46.773	124.06	11.936	25.52	0.6203	15.83
SM-200_mean	48.278	123.88	11.942	24.76	0.6194	15.34
B-35-g2-h30_S1	34.035	121.14	12.237	35.95	0.6057	22.15
B-35-g2-h30_S2	33.652	119.96	12.364	36.74	0.5998	22.04
B-35-g2-h30_S3	35.009	122.02	12.102	34.57	0.6101	21.09
B-35-g2-h30_mean	34.232	121.04	12.234	35.75	0.6052	21.76
AT200_S1	17.241	136.66	10.808	62.69	0.6833	42.83
AT200_S2	16.915	137.90	10.709	63.31	0.6895	43.65
AT200_S3	17.895	143.43	10.324	57.69	0.7172	41.37
AT200_mean	17.350	139.33	10.614	61.23	0.6967	42.62

Table 3.2. Change in crashworthiness indicators and maximum shortening for specimens with classic and innovative zone-annealed triggers compared to results for smooth columns.

Model	PCF	U_{max}	MCF	CLE	SE	TE
B-35-g2-h30_mean	-29.09%	-2.30%	2.45%	+44.41%	-2.30%	41.88%
AT200_mean	-64.06%	+12.47%	-11.13%	+147.30%	+12.47%	+177.89%

+ means an increase in relation to the smooth column
- means an decrease in relation to the smooth column

4. Final conclusions

Detailed conclusions are presented at the end of the previous chapter nevertheless it is worth summarising some final thoughts in general.

The experimental study has convincingly demonstrated the positive effect of the innovative ZAT trigger on the crashworthiness indicators of the energy absorber. A method for obtaining this type of trigger for specified column dimensions was presented. This method is still under development and is thus being standardized and improved. The paper also presented the novel method of making triggers in the form of concave and convex spherical indentations.

The calculations based on the crush force vs. shortening characteristics made it possible to quantify the yield obtained with the innovative trigger, and to compare the results with those obtained for the energy absorber with a trigger in the form of spherical indentations and the smooth one without any trigger. The energy absorber with ZAT was found to have significantly higher crashworthiness indicators.

In the near future, in addition to enhancing the method for obtaining reproducible and standardized columns with ZAT, research will be conducted on the properties of hybrid energy absorbers combining the features of the AT and B-35 models.

.

Reference

1. Abbasi M, Reddy S, Ghafari-Nazari A, Fard M. Multiobjective crashworthiness optimization of multi-cornered thin-walled sheet metal members. Thin-Walled Structures 2015; 89: 31–41, https://doi.org/10.1016/j.tws.2014.12.009.
2. Abramowicz W. Thin-walled structures as impact energy absorbers. Thin-Walled Structures, 2003; 41(2–3): 91–107, https://doi.org/10.1016/S0263-8231(02)00082-4.
3. Alavi Nia A, Parsapour M. Comparative analysis of energy absorption capacity of simple and multi-cell thin-walled tubes with triangular, square, hexagonal and octagonal sections. Thin-Walled Structures 2014; 74: 155–165, https://doi.org/10.1016/j.tws.2013.10.005.
4. Alghamdi A A A. Collapsible impact energy absorbers: An overview. Thin-Walled Structures 2001. doi:10.1016/S0263-8231(00)00048-3, https://doi.org/10.1016/S0263-8231(00)00048-3.
5. Ali M, Ohioma E, Kraft F, Alam K. Theoretical, numerical, and experimental study of dynamic axial crushing of thin walled pentagon and cross-shape tubes. Thin-Walled Structures 2015. doi:10.1016/j.tws.2015.04.007, https://doi.org/10.1016/j.tws.2015.04.007.
6. Baroutaji A, Sajjia M, Olabi A G. On the crashworthiness performance of thin-walled energy absorbers: Recent advances and future developments. Thin-Walled Structures 2017. doi:10.1016/j.tws.2017.05.018, https://doi.org/10.1016/j.tws.2017.05.018.
7. Chen W, Wierzbicki T. Relative merits of single-cell, multi-cell and foam-filled thin-walled structures in energy absorption. Thin-Walled Structures 2001. doi:10.1016/S0263-8231(01)00006-4, https://doi.org/10.1016/S0263-8231(01)00006-4.
8. Chien W Y, Pan J, Friedman P A. Failure prediction of aluminum laser-welded blanks. International Journal of Damage Mechanics 2003; 12(3): 193–223, https://doi.org/10.1177/1056789503012003002.
9. Deng X, Qin S, Huang J. Energy absorption characteristics of axially varying thickness lateral corrugated tubes under axial impact loading. Thin-Walled Structures 2021; 163(November 2020): 107721, https://doi.org/10.1016/j.tws.2021.107721.
10. Fang J, Sun G, Qiu N et al. On design optimization for structural crashworthiness and its state of the art. Structural and Multidisciplinary Optimization 2017; 55(3): 1091–1119, https://doi.org/10.1007/s00158-016-1579-y.
11. Ferdynus M, Gajewski J. Identification of crashworthiness indicators of column energy absorbers with triggers in the form of cylindrical

embossing on the lateral edges using artificial neural networks. Eksploatacja i Niezawodnosc 2022; 24(4): 805–821, https://doi.org/10.17531/ein.2022.4.20.
12. Ferdynus M, Rozylo P, Rogala M. Energy absorption capability of thin-walled prismatic aluminum tubes with spherical indentations. Materials 2020; 13(19): 1–19, https://doi.org/10.3390/ma13194304.
13. Ferdynus M, Szklarek K, Kotełko M. Crashworthiness performance of thin-walled hollow and foam-filled prismatic frusta, Part 2: Experimental study. Thin-Walled Structures 2022; 181(September): 110070, https://doi.org/10.1016/j.tws.2022.110070.
14. Gronostajski Z, Kaczyński P, Polak S, Bartczak B. Energy absorption of thin-walled profiles made of AZ31 magnesium alloy. Thin-Walled Structures 2018; 122(October 2017): 491–500, https://doi.org/10.1016/j.tws.2017.10.035.
15. Hanssen A G, Hopperstad O S, Langseth M. Design of aluminium foam-filled crash boxes of square and circular cross-sections. International Journal of Crashworthiness 2001; 6(2): 177–188, https://doi.org/10.1533/cras.2001.0171.
16. Hanssen A G, Langseth M, Hopperstad O S. Static and dynamic crushing of square aluminum extrusions with aluminum foam filler. International Journal of Impact Engineering 2000. doi:10.1016/S0734-743X(99)00169-4, https://doi.org/10.1016/S0734-743X(99)00169-4.
17. Jafarzadeh-Aghdam N, Schröder K U. Mechanism of reproducible axial impact of square crash boxes. Thin-Walled Structures 2022; 176(February): 109062, https://doi.org/10.1016/j.tws.2022.109062.
18. Jandaghi Shahi V, Marzbanrad J. Analytical and experimental studies on quasi-static axial crush behavior of thin-walled tailor-made aluminum tubes. Thin-Walled Structures 2012; 60: 24–37, https://doi.org/10.1016/j.tws.2012.05.015.
19. Jaśkiewicz M. Evaluation of the Reliability of the Shoulder and Knee Joint of the KPSIT C50 Dummy Adapted to Crash tests carried out at low speeds. Eksploatacja i Niezawodnosc 2024; 26(1): 0–2, https://doi.org/10.17531/ein/178376.
20. Jones N. Structural Impact. 1990. doi:10.1017/cbo9780511624285, https://doi.org/10.1017/cbo9780511624285.
21. Karagiozova D, Jones N. Dynamic buckling of elastic-plastic square tubes under axial impact - II: Structural response. International Journal of Impact Engineering 2004; 30(2): 167–192, https://doi.org/10.1016/S0734-743X(03)00062-9.
22. Kotełko M, Ferdynus M, Jankowski J. Energy absorbing effectiveness- different approaches. Acta Mechanica et Automatica 2018; 12: 54–59.
23. Kozłowski E, Borucka A, Oleszczuk P, Jałowiec T. Evaluation of the maintenance system readiness using the semi-Markov model taking into account hidden factors. Eksploatacja i Niezawodnosc 2023; 25(4): 0–2, https://doi.org/10.17531/ein/172857.
24. Langseth M, Hopperstad O S. Static and dynamic axial crushing of square thin-walled aluminium extrusions. International Journal of Impact Engineering 1996. doi:10.1016/s0734-743x(96)00025-5, https://doi.org/10.1016/s0734-743x(96)00025-5.
25. Lee S, Hahn C, Rhee M, Oh J E. Effect of triggering on the energy absorption capacity of axially compressed aluminum tubes. Materials and Design 1999; 20(1): 31–40, https://doi.org/10.1016/s0261-3069(98)00043-0.
26. M.Rogala, J.Gajewski, M.Ferdynus. The Effect of Geometrical Non-Linearity on the Crashworthiness of Thin-Walled Conical Energy-Absorbers. Materials 2020. doi:10.3390/ma13214857, https://doi.org/10.3390/ma13214857.
27. Merklein M, Böhm W, Lechner M. Tailoring Material Properties of Aluminum by Local Laser Heat Treatment. Physics Procedia 2012; 39: 232–239, https://doi.org/10.1016/j.phpro.2012.10.034.
28. Merklein M, Johannes M, Lechner M, Kuppert A. A review on tailored blanks - Production, applications and evaluation. Journal of Materials Processing Technology 2014; 214(2): 151–164, https://doi.org/10.1016/j.jmatprotec.2013.08.015.
29. Nia A A, Hamedani J H. Comparative analysis of energy absorption and deformations of thin walled tubes with various section geometries. Thin-Walled Structures 2010. doi:10.1016/j.tws.2010.07.003, https://doi.org/10.1016/j.tws.2010.07.003.
30. Peixinho N, Soares D, Vilarinho C et al. Experimental study of impact energy absorption in aluminium square tubes with thermal triggers. Materials Research 2012; 15(2): 323–332, https://doi.org/10.1590/S1516-14392012005000011.
31. Ptak M, Wilhelm J, Sawicki M et al. Assessment of child safety on bicycles in baby carriers – The importance of evaluating both head and neck injuries. Journal of Safety Research 2023; 85(78): 254–265, https://doi.org/10.1016/j.jsr.2023.02.009.
32. Rai V, Ghasemnejad H, Watson J W et al. Developed trigger mechanisms to improve crush force efficiency of aluminium tubes. Engineering Structures 2019; 199(April): 109620, https://doi.org/10.1016/j.engstruct.2019.109620.
33. Reddy S, Abbasi M, Fard M. Multi-cornered thin-walled sheet metal members for enhanced crashworthiness and occupant protection. Thin-Walled Structures 2015. doi:10.1016/j.tws.2015.03.029, https://doi.org/10.1016/j.tws.2015.03.029.
34. Shakeri H R, Buste A, Worswick M J et al. Study of damage initiation and fracture in aluminum tailor welded blanks made via different welding

techniques. Journal of Light Metals 2002; 2(2): 95–110, https://doi.org/https://doi.org/10.1016/S1471-5317(02)00028-7.

35. Sharifi S, Shakeri M, Fakhari H E, Bodaghi M. Experimental investigation of bitubal circular energy absorbers under quasi-static axial load. Thin-Walled Structures 2015. doi:10.1016/j.tws.2014.12.008, https://doi.org/10.1016/j.tws.2014.12.008.
36. Xu F. Enhancing material efficiency of energy absorbers through graded thickness structures. Thin-Walled Structures 2015; 97: 250–265, https://doi.org/10.1016/j.tws.2015.09.020.
37. Xu F, Zhang X, Zhang H. A review on functionally graded structures and materials for energy absorption. Engineering Structures 2018; 171(February): 309–325, https://doi.org/10.1016/j.engstruct.2018.05.094.
38. Yao R, Pang T, Zhang B et al. On the crashworthiness of thin-walled multi-cell structures and materials: State of the art and prospects. Thin-Walled Structures 2023; 189(February): 110734, https://doi.org/10.1016/j.tws.2023.110734.
39. Ying L, Wang S, Gao T et al. Crashworthiness analysis and optimization of multi-functional gradient foam-aluminum filled hierarchical thin-walled structures. Thin-Walled Structures 2023; 189(February): 110906, https://doi.org/10.1016/j.tws.2023.110906.
40. Yuen S C K, Nurick G N. The energy-absorbing characteristics of tubular structures with geometric and material modifications: An overview. Applied Mechanics Reviews 2008; 61(1–6): 0208021–02080215, https://doi.org/10.1115/1.2885138.
41. Zhang X, Cheng G, Wang B, Zhang H. Optimum design for energy absorption of bitubal hexagonal columns with honeycomb core. International Journal of Crashworthiness 2008; 13(1): 99–107, https://doi.org/10.1080/13588260701731732.
42. Zhang X, Cheng G, Zhang H. Numerical investigations on a new type of energy-absorbing structure based on free inversion of tubes. International Journal of Mechanical Sciences 2009; 51(1): 64–76, https://doi.org/10.1016/j.ijmecsci.2008.11.001.
43. Zhang X, Zhang H, Wen Z. Axial crushing of tapered circular tubes with graded thickness. International Journal of Mechanical Sciences 2015. doi:10.1016/j.ijmecsci.2014.11.022, https://doi.org/10.1016/j.ijmecsci.2014.11.022.